Real-time two-dimensional surface profile measurement in a sinusoidal phase-modulating laser diode interferometer

Takamasa Suzuki
Osami Sasaki
Jinsaku Kaneda
Takeo Maruyama
Niigata University
Faculty of Engineering
8050 Ikarashi 2
Niigata-shi 950-21, Japan

Abstract. A real-time 2-D surface profile measurement system is described. In this system, a laser diode and a 2-D charge-coupled device image sensor are used as a light source and a photodetector, respectively. The phase is detected from the sinusoidal phase-modulating interference signal using the high-speed electrical circuit. The time required for phase detection is 20 ms for 50×40 measuring points. Because the phases can be obtained for even and odd fields of the image sensor, the original spatial resolution of the image sensor is not reduced in this system. Repeatability of the measurement is ~ 14 nm, rms.

Subject terms: interferometer; laser diode; sinusoidal phase modulating; image sensor.

Optical Engineering 33(8), 2754–2759 (August 1994).

1 Introduction

The exact 2-D surface profile of an object is needed in many fields, such as defect inspection in precision manufacturing. In such fields, the optical interferometer is popular and has been often used for a long time because it is a precise noncontacting method. The most popular is the heterodyne interferometer,[1,2] which utilizes frequency shift technology. In such interferometers, the phase detection is implemented easily using an electrical phase detector, and real-time measurement systems have been proposed.[3–5] The system described in Ref. 5, for example, obtained a serial data acquisition rate of 50 μs/point; a phase accuracy of λ/70 rms, where $\lambda = 647.1$ nm was a wavelength of the Kr ion laser; and a spatial resolution of 100 μm. But they need a frequency shifter, such as a Bragg cell, so the optical system is complicated in structure.

Recently, laser diodes (LDs) have been applied to interferometry[6–8] in place of the gas laser. The use of LDs is increasing because of their improved performance. The LD interferometer has some attractive features. For example, it can be constructed compactly, the phase modulation is easily performed, and external disturbance can be eliminated by controlling LD injection current[9,10] with feedback. However, it is necessary to implement phase calculation in LD interferometer because rather than frequency shift technology it uses phase shift technology for a modulating process. In the past, most of the LD interferometers used a computer for phase calculation so that the time for phase detection was not significant. Namely, signal processing has generally been performed in the conventional way. In the case of 2-D profiling, however, the number of measuring points becomes so large that the calculation time cannot be ignored. This is undesirable for manufacturing inspection. Therefore, the LD interferometer needs to be able to implement real-time phase detection. We have also utilized LDs for sinusoidal phase-modulating (SPM) interferometry[11,12] and have investigated the real-time signal processing for vibration measurement[13,14] and 1-D surface profiling[15–17] using an exclusive circuit or feedback control.

In this paper, we describe a real-time 2-D surface profile measurement system (SPMS) that succeeds that research. Because we use SPM LD interferometry, the principle of phase detection in our SPMS is the same as in Ref. 12, but all the calculations for phase detection are performed by an electrical circuit without a computer. It obtains a serial data acquisition rate of 10 μs/point; measurement repeatability of $\sim \lambda/60$, where $\lambda = 780$ nm is a wavelength of the LD; and spatial resolution of ~ 5 μm.

We use a 2-D charge-coupled device (CCD) image sensor as a photodetector. The signals obtained by the 2-D CCD image sensor are taken out at the even and the odd fields alternately. In the past, because the timing condition for the phase calculation cannot be satisfied in both fields, only one field was used[7] for phase detection. Therefore, the ability of spatial resolution was reduced by half compared with the original resolution of the CCD image sensor. To overcome this problem, we made a timing controller to deal with the signals of both fields. The principle of phase detection is described in Sec. 2. The implementation and time sequence of the electrical circuit in the SPMS are shown in Sec. 3. Experimental results are shown in Sec. 4.

Paper 26073 received Jul. 27, 1993; revised manuscript received Dec. 10, 1993; accepted for publication Dec. 11, 1993.

2 Principle of the Real-Time Surface Profile Measurement

2.1 *Optical System*

The setup of an SPM LD interferometer for real-time 2-D surface profile measurement is shown in Fig. 1. We use a Twyman-Green interferometer whose optical path difference between reference mirror M and an object is $2D_0$. A dc bias current I_0 and a modulation current $I_m(t)$ generated by a sinusoidal oscillator are injected into the LD by a LD modulator LM, where $I_m(t)$ is given by

$$I_m(t) = a\ \cos(\omega_c t + \theta)\ . \tag{1}$$

Then the SPM interference signal $S(t,x,y)$ is obtained as

$$S(t,x,y) = S_{dc} + S_0\ \cos[-z\ \cos(\omega_c t + \theta) + \alpha(x,y)]\ , \tag{2}$$

where

$$z = \frac{4\pi a \beta D_0}{\lambda_0}\ , \tag{3}$$

$$\alpha(x,y) = \frac{4\pi\ d(x,y)}{\lambda_0}\ , \tag{4}$$

where β is a modulation efficiency of the LD; λ_0 is the LD central wavelength, which is determined by the dc bias current I_0; and $d(x,y)$ represents a surface profile of the object. An interference signal $S(t,x,y)$ is imaged onto the 2-D CCD image sensor with lens L2. The unused pixels on the CCD image sensor are masked with black paper. Because we have no need to read the covered pixels, readout time for the CCD image sensor can be reduced. The masked area on the CCD image sensor is determined by the charge storage period and readout time for each pixel.

2.2 *Principle of the Phase Detection*

The readout timing for the CCD image sensor is briefly shown in Fig. 2. Figure 2(a) shows a modulation signal $I_m(t)$. The readout reference pulse (Pr) for the CCD image sensor is shown in Fig. 2(b). Because the charge storage period T_c of the CCD image sensor is selected as $T/4$, we obtain the four integrated values $p_i(x,y)$ $(i = 1 \sim 4)$ in a period of $I_m(t)$, as shown in Fig. 2(c), where $T = 2\pi/\omega_c$. The readout period of the CCD image sensor is shown in Fig. 2(d). The signals p_i are read out after the completion of integration. The readout period for each integrated value is $T_c/2$. The remaining period of $T_c/2$ is used for the other field. Although the signals are obtained alternately for the even and odd fields in the 2-D CCD image sensor, we show the signals only for one field in Fig. 2(d) to simplify the explanations. The control timing for the CCD image sensor is explained in more detail in Sec. 4. The signals $p_i(x,y)$ are the integrated value of $S(t,x,y)$. They are given by

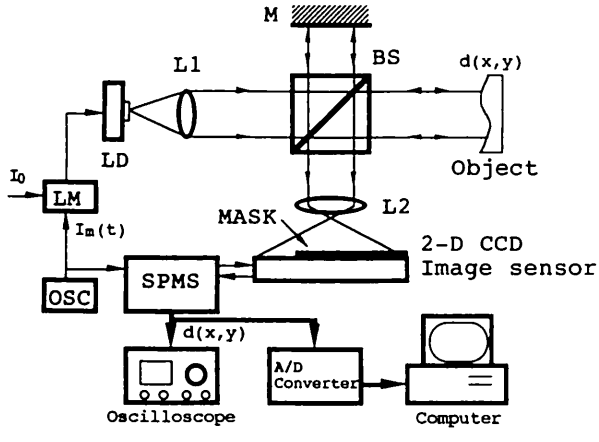

Fig. 1 Experimental setup of an SPM LD interferometer for real-time 2-D surface profile measurement. The surface profile $d(x,y)$ of the object is calculated from the interference signal by an SPMS.

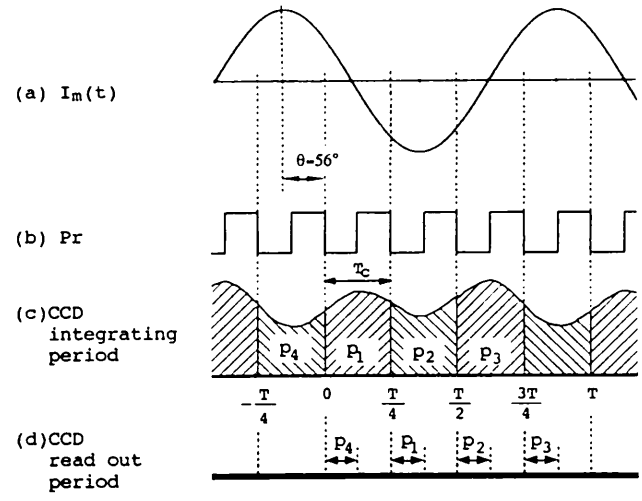

Fig. 2 Readout timing for the CCD image sensor: (a) modulation signal $I_m(t)$; (b) reference pulse (Pr), which is delayed by 56 deg in phase; (c) the integrating period of the CCD image sensor homeomorphic to Pr; and (d) the readout period of the CCD image sensor.

$$p_i(x,y) = \int_{(T/4)(i-1)}^{(T/4)i} S(t,x,y)\ dt\ , \tag{5}$$

where $T = 2\pi/\omega_c$ and x and y denote the coordinates of the 2-D surface of the object. Calculating Eq. (5) and taking addition and subtraction for each pixel, we obtain[12]

$$P_c(x,y) = -p_4 + p_1 - p_2 + p_3 = A_c\ \cos\alpha(x,y)\ , \tag{6}$$

$$P_s(x,y) = -p_4 + p_1 + p_2 - p_3 = A_s\ \sin\alpha(x,y)\ , \tag{7}$$

where A_c and A_s are the functions of z and θ. They are given by

$$A_c = (8/\pi) \sum_{n=1}^{\infty} [J_{2n}(z)/2n][1 - (-1)^n]\ \sin(2n\theta)\ , \tag{8}$$

$$A_s = (8/\pi) \sum_{n=1}^{\infty} [J_{2n-1}(z)/2(n-1)](-1)^n\ \sin[(2n-1)\theta]\ , \tag{9}$$

and $J_n(z)$ is an n'th-order Bessel function. Figure 3 shows A_c and A_s calculated from Eqs. (8) and (9) for θ, where z is

selected as an optimum value[12] 2.45. When the parameters z and θ are selected as 2.45 and 56 deg, respectively, the condition $A_c = A_s$ is achieved and the phase $\alpha(x,y)$ is calculated by

$$\alpha(x,y) = \tan^{-1}[P_s(x,y)/P_c(x,y)] \quad . \tag{10}$$

From Eqs. (4) and (10), the surface profile is calculated by

$$d(x,y) = [\lambda/(4\pi)] \tan^{-1}(P_s/P_c) \quad . \tag{11}$$

The detected surface profile $d(x,y)$ can be observed by an oscilloscope in real time or displayed in 3-D graphics using an analog-to-digital (A/D) converter and a computer. The computer is used only for 3-D graphic display.

3 Configuration and Implementation of the System

The block diagram of the SPMS is shown in Fig. 4. It has an A/D converter, two operational circuits, a read only memory (ROM), and a digital-to-analog (D/A) converter. The operational circuit consists of a sign changer, an adder, and random access memory (RAM). The table in Fig. 4 shows the operations corresponding to the addition and subtraction (ADD/SUB) signal. The output of the CCD image sensor is converted to 8-bit digital signal by an A/D converter and fed into an operational circuit in which the calculations based on Eqs. (6) and (7) are implemented.

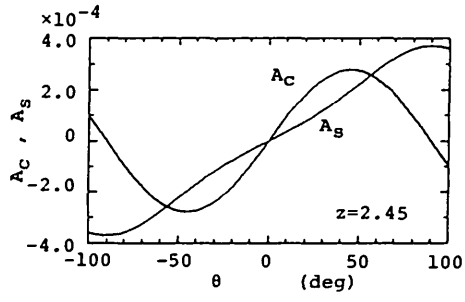

Fig. 3 Amplitudes of $\cos\alpha(x,y)$ and $\sin\alpha(x,y)$ calculated from Eqs. (8) and (9) for $-100 \text{ deg} \leq \theta \leq 100$ deg, where z was selected as an optimum value 2.45.

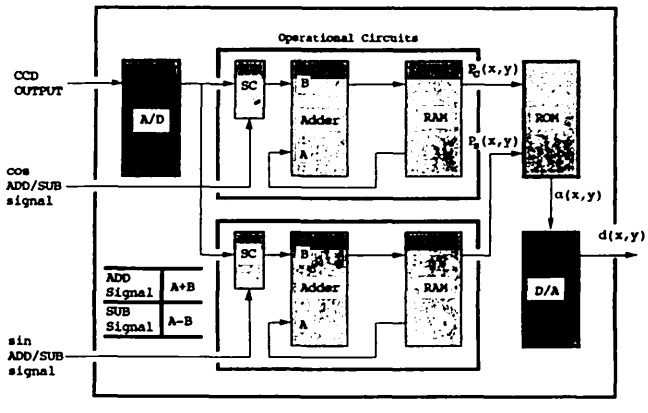

Fig. 4 Block diagram of the SPMS. The inset of table shows the operation corresponding to the addition and subtraction (ADD/SUB) signal.

The operational process for $P_c(x,y)$ is explained in detail in Fig. 5, where the coordinates (x,y) are omitted. Because the addition or subtraction is implemented alternately to avoid the overflow that comes from the existence of dc offset S_{dc} in $S(t,x,y)$, the operation begins with $-p_4$, as shown in Eqs. (6) and (7).

First, as shown in Fig. 5(a), $-p_4$ is obtained and written to RAM between $t=0$ and $T/4$ for all the sampling points. Next, p_1, taken from the CCD image sensor, and $-p_4$, read from RAM, are added and written to RAM again. Then $-p_4+p_1$ is obtained between $t=T/4$ and $T/2$. Third, p_2 is subtracted from $-p_4+p_1$ between $t=T/2$ and $3T/4$. Finally, between $t=3T/4$ and T, $-p_4+p_1-p_2+p_3=P_c(x,y)$ is obtained for all coordinates x and y. The operational process for $P_s(x,y)$ is the same as for $P_c(x,y)$ except for the order of addition and subtraction. Then all the $P_c(x,y)$'s and $P_s(x,y)$'s are obtained as an 8-bit digital value. The digital values of $P_c(x,y)$ and $P_s(x,y)$ are used as a column address and a row address, respectively, for ROM, in which $\alpha(x,y)$'s or $\tan^{-1}(P_s/P_c)$'s have been calculated in advance for all combinations of P_c and P_s and stored in the address designated by the digital values of P_c and P_s. The region of $\alpha(x,y)$ is 0 to 2π rad. The details of ROM contents are the same as those in Ref. 12. The digital signal $\alpha(x,y)$ is fed into the D/A converter and converted to an analog signal or surface profile $d(x,y)$.

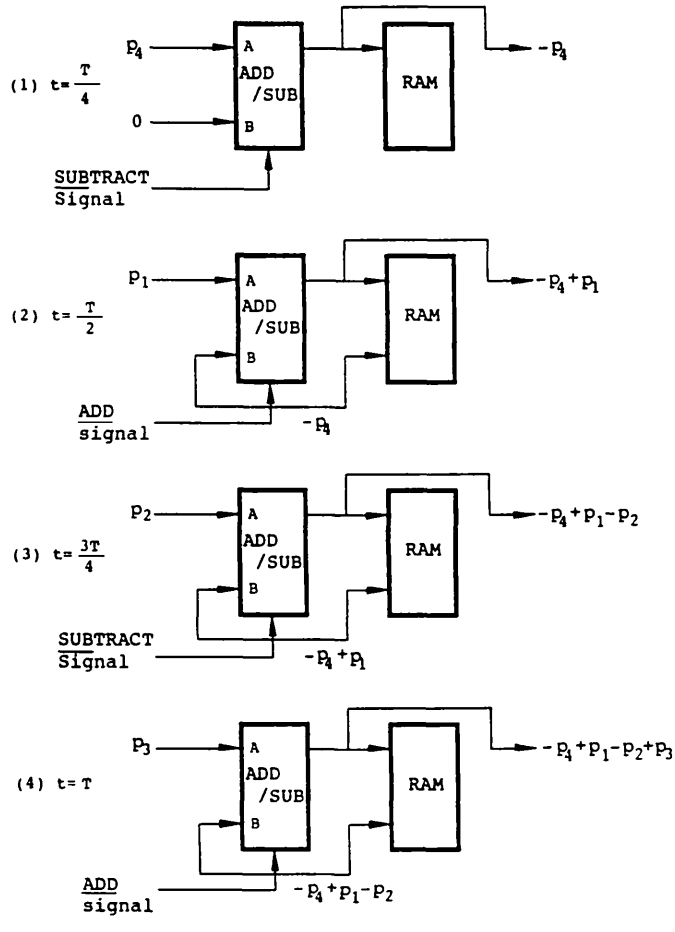

Fig. 5 Explanation of the operations in the SPMS. A cycle of the operation begins with p_4 and ends with p_3 to avoid the overflow.

4 Control Timing for the CCD Image Sensor

We used an interline-transfer-type of 2-D CCD image sensor as a photodetector. It was driven by a frame-storage-drive mode, which is most commonly used for a video camera. Thus, the interference signal integrated in the even and odd fields is taken out alternately from the CCD image sensor. The control timing of the CCD image sensor is precisely shown in Fig. 6. Figures 6(a), 6(b), and 6(c) are modulation signal $I_m(t)$, readout reference pulse Pr, and interference signal $S(t)$, respectively, which are already shown in Fig. 2. The interference signal is integrated in the even and odd fields. The integrating periods are shown in Figs. 6(d) and 6(e). Although the integrating period for the even and odd fields are overlapped, the charge storages in each field are read out serially, as shown in Fig. 6(f). For example, the interference signal integrated in the region of E_{14} is read out from the CCD image sensor in the region of [a] in Fig. 6(f). In the same way, the interference signal integrated in the region of O_{14} is read out in the region of [b] in Fig. 6(f). Because the signals E_{14}, E_{11}, E_{12}, and E_{13} correspond to p_4, p_1, p_2, and p_3 in Fig. 2, respectively, the surface profile can be obtained in the region of (A2) for the signals in the even field. But the condition $A_c = A_s$ is not satisfied for the signals O_{1i} ($i = 1 \sim 4$) in the odd field ($\theta = 101$ deg), so the surface profile cannot be obtained in the region of (A2). To overcome this problem, we controlled the integrating period at the end of the region of (A2). That is, we extend the period of E_{24} by half and shorten the period of O_{24} by half. Then the odd field is delayed by 56 deg in the regions of (B1) and (B2). In the region of (B1), however, the signal O_{24} is inaccurate, so the calculation is implemented only in the region of (B2). In the region of (B2), the charge storages integrated in the region of O_{34} and E_{34} are read out from the CCD image sensor in the region of [c] and [d], respectively. Consequently the surface profile can be obtained for both fields in the regions of (A2) and (B2). At the end of the region of (B2), the period of E_{44} is shortened and the period of O_{44} is extended to restore the integrating timing. The surface profile for each field of the CCD image sensor is obtained every four periods of $I_m(t)$ or every period of $4T$. If the surface profile for only one field is adequate, however, the measurement time for the phase detection becomes T.

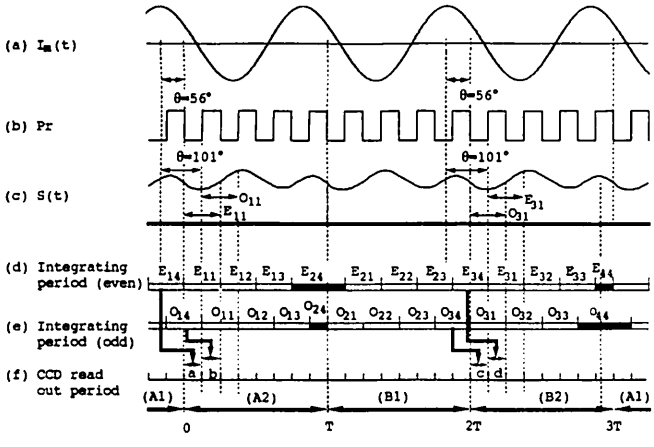

Fig. 6 Control timing of the CCD image sensor: (a) modulation signal $I_m(t)$; (b) reference pulse Pr; (c) interference signal $S(t)$; (d) and (e) the integrating period for even and odd field, respectively; and (f) the readout period of the CCD image sensor. The surface profiles for even and odd field are detected in the regions of (A2) and (B2), respectively.

5 Experiments

The experimental setup is shown in Fig. 1. The optical path difference $2D_0$ is 100 mm. The light source is a GaAlAs LD (HITACH HL7801E), whose central wavelength is 780 nm and maximum output power is 5 mW. The modulation frequency $\omega_c/2\pi$ for the LD is 200 Hz. Consequently, the frequency for the phase detection in both fields is 50 Hz, or the measurement time is 20 ms. If only the one field is adequate, the time becomes 5 ms. The photodetector is an interline type of 2-D CCD image sensor (SONY ICX-018CL). It has 510(H)×492(V) pixels, where H indicates horizontal and V vertical, but we used a part of them by masking with a black paper. The size of 1 pixel is 17(H)×13(V) μm. The readout frequency for each pixel was 4 MHz, or 0.25 μs. Because the modulation frequency is 200 Hz, the period of charge storage is 1.25 ms and the readout time for one field is 0.625 ms, which is a half of the period of charge storage, as shown in Fig. 6(f). The operation at each stage shown in Fig. 5 must be completed in the readout time 0.625 ms for all pixels. The maximum number of measurable points is calculated as 0.625 ms/0.25 μs = 2500. But the number of the effective pixels becomes ~1000 by the existence of dummy bits, blanking period, and inaccurate signals detected near the edge of masking paper. Then the number of effective pixels in both fields is ~2000 = ~50×40 and the serial data acquisition rate becomes 20 ms/2000 = 10 μs/point. To satisfy the condition $A_c = A_s$, the phase of Pr was shifted by 56 deg and z was set to 2.45 by adjusting the amplitude of the modulation current.

First, to check our system, we measured the surface profile of the mirror. The measurement result is shown in Fig. 7. The magnification of L2 was 1 and the spatial interval of the measuring points was 17(H)×13(V) μm. The mirror was placed perpendicularly against the incident beam by monitoring the oscilloscope. We confirmed that the 2-D surface profile of 50×40 pixels could be measured in real time.

Next, we measured the surface profile of a diamond-turned aluminium disk, whose cutting pitch is ~50 μm. The 1-D surface profile measured by a Talystep instrument is shown

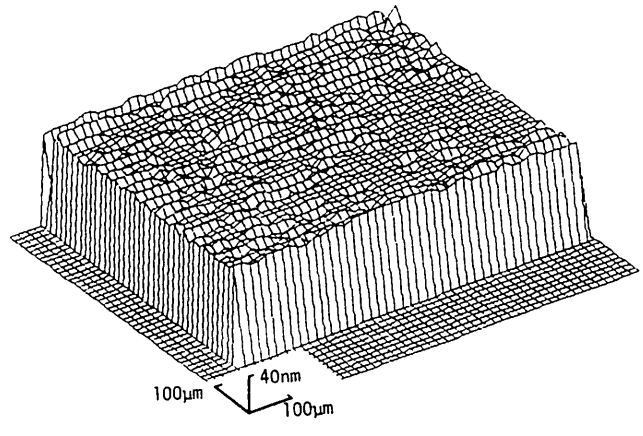

Fig. 7 Surface profile of the mirror measured by our system in real time.

in Fig. 8. The surface roughness is ~100 nm and the cutting pitch was measured accurately. It shows that the surface profile of the disk has a periodic structure determined by a cutting pitch. The surface profile measured by our system is shown in Fig. 9. Because the magnification of L2 was 3, the spatial interval of the measuring points was ~5.7(H)×4.3(V) μm. The measured area was not the same as that of Fig. 8. The displayed area is limited to 40(H)×20(V) to obtain the conspicuous profile. The roughness and the cutting pitch shown in Fig. 9(a) agree well with the profile shown in Fig. 8. The same area of the same disk was measured after a few minutes, and the result is shown in Fig. 9(b). Figures 9(a) and 9(b) agree well. We attempted to calculate the repeatability of the measurement from Figs. 9(a) and 9(b); that is, we subtracted the profile in Fig. 9(b) from that in Fig. 9(a) for each corresponding pixel and calculated the root-mean-square (rms) value. As a result, the repeated measurement error is estimated to be ~14 nm rms and is equivalent to ~λ/60. This error contains external disturbances and we think the feedback control would be effective[10] to improve the repeatability of measurement.

6 Conclusions

We proposed and demonstrated a real-time 2-D surface profile measurement system. The time required for the measurement was 20 ms in this demonstration, but it can be reduced to a quarter, or 5 ms, when only the one field of the 2-D CCD image sensor is used for the measurement. Moreover, if the operational frequency could be higher, the measurement time would be reduced.

Because the experimental setup is made up with general-purpose digital integrated circuits, it is adequate to check the operational process at each part of the circuit. But if most of the circuit including the CCD driver could be replaced by a digital signal processor or programmable array logic, the reliability and the performance—for example, the time for implementation or miniaturization—would be improved.

References

1. R. Crane, "Interference phase measurement," *Appl. Opt.* **8**(3), 538–542 (1969).
2. G. E. Sommargren and B. J. Thompson, "Linear phase microscopy," *Appl. Opt.* **12**(9), 2130–2138 (1973).
3. K. D. Stumpf, "Real-time interferometer," *Opt. Eng.* **18**, 648–653 (1979).
4. N. A. Massie, R. D. Nelson, and S. Holly, "High-performance real-time heterodyne interferometry," *Appl. Opt.* **18**(11), 1797–1803 (1979).
5. N. A. Massie, "Real-time digital heterodyne interferometry: a system," *Appl. Opt.* **19**(1), 154–160 (1980).

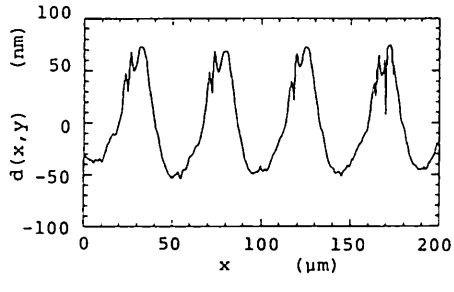

Fig. 8 Surface profile of a diamond-turned aluminium disk measured by a Talystep instrument.

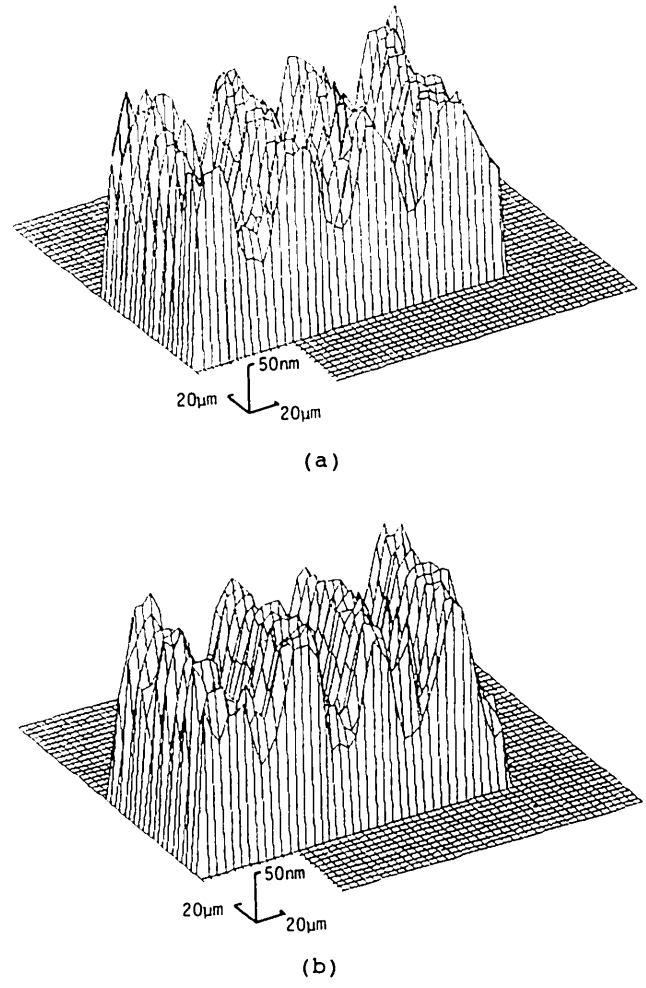

Fig. 9 Experimental results measured by our system: (a) surface profile of the same disk shown in Fig. 8 and (b) surface profile ob-

6. K. Tatsuno and Y. Tsunoda, "Diode laser direct modulation heterodyne interferometer," *Appl. Opt.* **26**(1), 37–40 (1987).
7. J. Chen, Y. Ishii, and K. Murata, "Heterodyne interferometry with a frequency-modulated laser diode," *Appl. Opt.* **27**(1), 124–128 (1988).
8. K. Hotate and D.-T. Jong, "Quasiheterodyne optical fiber sensor with automated adjustment of the driving wave parameter," *Appl. Opt.* **26**(15), 2956–2961 (1987).
9. T. Yoshino, M. Nara, S. Mnatzakanian, B. S. Lee, and T. C. Strand, "Laser diode feedback interferometer for stabilization and displace measurement," *Appl. Opt.* **26**(5), 892–897 (1987).
10. O. Sasaki, T. Takahashi, and T. Suzuki, "Sinusoidal phase modulating laser diode interferometer with a feedback control system to eliminate external disturbance," *Opt. Eng.* **29**(12), 1511–1515 (1990).
11. O. Sasaki and H. Okazaki, "Sinusoidal phase modulating interferometry for surface profile measurement," *Appl. Opt.* **25**(18), 3137–3140 (1986).
12. O. Sasaki, H. Okazaki, and M. Sakai, "Sinusoidal phase modulating interferometer using the integrating-bucket method," *Appl. Opt.* **26**(6), 1089–1093 (1987).
13. T. Suzuki, O. Sasaki, T. Higuchi, and T. Maruyama, "Real time displacement measurement in sinusoidal phase modulating interferometry," *Appl. Opt.* **28**(24), 5270–5274 (1989).
14. T. Suzuki, O. Sasaki, S. Takayama, and T. Maruyama, "Real-time displacement measurement using synchronous detection in a sinusoidal phase modulating interferometer," *Opt. Eng.* **32**(5), 1033–1037 (1993).
15. T. Suzuki, O. Sasaki, and T. Maruyama, "Phase locked laser diode interferometry for surface profile measurement," *Appl. Opt.* **28**(20), 4407–4410 (1989).
16. T. Suzuki, O. Sasaki, K. Higuchi, and T. Maruyama, "Phase locked laser diode interferometer: high speed feedback control system," *Appl. Opt.* **30**(25), 3622–3626 (1991).
17. T. Suzuki, O. Sasaki, K. Higuchi, and T. Maruyama, "Differential type of phase-locked laser diode interferometer free from external disturbance," *Appl. Opt.* **31**(34), 7242–7248 (1992).

Takamasa Suzuki received the BE degree from Niigata University in 1982, the ME degree from Touhoku University in 1984 and the DrE degree from Tokyo Institute of Technology in 1994, all in electrical engineering. He is an associate professor in the Department of Electrical and Electronic Engineering at Niigata University. Since 1987 he has worked on interferometers using laser diodes and applications of phase conjugate optics at Niigata University.

Osami Sasaki received the BE and ME degrees in electrical engineering from Niigata University in 1972 and 1974, respectively, and the DrE degree in electrical engineering from Tokyo Institute of Technology in 1981 and is a professor in the Department of Electrical and Electronic Engineering at Niigata University. Since 1974 he has worked in the field of optical measuring systems and optical information processing.

Jinsaku Kaneda received the BE degree in electrical engineering from Niigata University in 1993. He has been involved with sinusoidal phase modulating interferometers. Since 1993 he has worked on the development of a monitor TV system at Matsushita Electric Industrial Corporation.

Takeo Maruyama received the BE degree in electrical engineering from Niigata University in 1965 and the DrE degree in electrical engineering from Nagoya University in 1979, and is a professor in the Department of Electrical and Electronic Engineering at Niigata University. Since 1965 he has worked in the field of the physics of ionized gases and optical metrology.